Supporting Online Material for

Orbital-Independent Superconducting Gaps in Iron-Pnictides

T. Shimojima,* F. Sakaguchi, K. Ishizaka, Y. Ishida, T. Kiss, M. Okawa, T. Togashi, C.-T. Chen, S. Watanabe, M. Arita, K. Shimada, H. Namatame, M. Taniguchi, K. Ohgushi, S. Kasahara, T. Terashima, T. Shibauchi, Y. Matsuda, A. Chainani, S. Shin*

*To whom correspondence should be addressed.
E-mail: shimojima@ap.t.u-tokyo.ac.jp (T.S); shin@issp.u-tokyo.ac.jp (S.S.)

Published 7 April 2011 on *Science* Express
DOI: 10.1126/science.1202150

This PDF file includes:

Supporting Online Text and Figures

1. Materials and Methods

The electronic structure in iron-pnictides is highly sensitive to the crystal structure, particularly in relation to pnictogen height relative to the iron plane (S1). At the crystal surface cleaved for ARPES, not only the pnictogen height but also carrier concentration might be different from that of the bulk single crystal. These effects modify the electronic structure, so a bulk-sensitive light source is indispensable for ARPES on iron-pnictides. The vacuum ultraviolet laser ($h\nu$ = 7 eV) leads to electron emission from ~10 conducting layers (~ 100 Å) below the surface, in contrast to the typical photoelectron escape depth of ~ 1 Å in previous ARPES (S2).

Laser-ARPES measurements were performed on a spectrometer built using a VG-Scienta R4000WAL electron analyzer and a VUV-laser of 6.994 eV as a photon source. (S3) Using the λ/2 (half-wave) plate, we can rotate the light polarization vector and obtain *s*- or *p*-polarized light without changing the optical path. The energy resolution was set to 3 meV to get high count rate. The spectra were reproducible over measurement cycles of 4 hours. E_F of samples was referenced to that of gold film evaporated onto the sample substrate. All measurements were done on surfaces cleaved at 150 K in ultra high vacuum better that 5×10^{-11} Torr. Single crystals of $Ba_{0.59}K_{0.41}Fe_2As_2$ and $BaFe_2(As_{0.65}P_{0.35})_2$ were grown by the self-flux method as described in detail in Ref. S4 and Ref. S5.

2. Determination of the SC gap magnitude using BCS spectral function

SC gap magnitude was quantitatively determined by the similar method of Ref. S6. BCS spectral function of the form

$$A_{BCS}(k,\omega)=\frac{1}{\pi}\left\{\frac{|u_k|^2\Gamma}{(\omega-E_k)^2+\Gamma^2}+\frac{|v_k|^2\Gamma}{(\omega+E_k)^2+\Gamma^2}\right\},\quad E_k=\left[\varepsilon_k{}^2+|\Delta(k)|^2\right]^{1/2}$$

was used, where $|u_k|^2$ and $|v_k|^2$ are coherence factors, Γ line width broadening factor due to the finite quasiparticle lifetime, E_k Bogoliubov quasiparticle band dispersion, ε_k band dispersion near E_F in the normal state, Δ(k) SC gap magnitude. In order to obtain the fitting function, BCS spectral function is multiplied by Fermi Dirac function and convoluted with Gaussian corresponding to the experimental energy resolution. We also used Shirley-type background. Momentum width integrated to obtain the EDC is taken into account. Then, obtained fitting function can be used to reproduce the EDCs in order to quantitatively determine Δ(k). Sometimes Δ(k) has been estimated from the binding energy of SC peak position in the EDCs. However such analysis leads to overestimation of the gap magnitude when the spectrum is rather broad like iron-pnictides.

3. Origin of the peak 2 in the EDCs for BaK122

In order to investigate the origin of the peak 2, we take a close look at its *T*-dependence across T_c. Peak 2 shows small energy shift of ~ 3 meV below T_c as if tracing the evolution of peak 1(Fig.3 **F**). Remarkably, peak 2 survives even above T_c as seen in the divided EDCs up to ~ 90 K (Fig.S1 **A**). If peak 2 originated in the superconductivity, possible explanation for the peak to remain in the normal state is

pseudo-gap formation smoothly connecting to the SC gap as observed in copper oxides (S7,S8). If this is the case, peaks above T_c are then expected to develop in both occupied and unoccupied states as a precursor of SC peaks, concomitantly forming a pseudogap structure at E_F. However, this scenario is ruled out for BaK122 since we observe no reduction of intensity at E_F on cooling in the normal state (Fig.S1 **B**). In addition, peak 2 is detected only in occupied states as shown in the spectra at 60 K or 90 K in Fig. S1**A**. These results indicate that peak 2 is not directly interpreted as a SC peak. The complex spectral features are summarized in the schematics in supplementary Fig. S1 **A**. The SC gap (blue) opens below T_c at the slope of the mysterious peak 2 (red).

A candidate for the origin of the peak 2 is magnetic resonance mode observed by inelastic neutron scattering (INS) measurement (S9). Recent calculation on the partial density of state considering spin fluctuation shows a resonance-like peak evolution just below E_F in hole doped system (S10). Since the peak 2 is not observed in AsP122, comparative INS studies on BaK122 and AsP122 are required for elucidating the origin of the peak 2.

Another candidate is a coupling mode related to the orbital degrees of freedom. Recent ARPES on detwinned FeCo122 reported that anisotropic orbital occupancy of zx/yz orbitals starts at a higher temperature above T_N and T_S. (S11). The T-dependence is similar to that of peak 2 in the Fig.S1. Nevertheless, systematic investigations on the material dependence of the anisotropic orbital occupation are further required to conclude this issue.

4. **Small SC gap magnitude in the hole FSs**.

Nearly equivalent magnitude of the SC gaps in three hole FSs is a common feature among optimally-doped AsP122 and BaK122 near $k_z = \pi$. We obtain the reduced gap value $2\Delta/k_BT_c \sim 1.7$ and ~ 3.0 for BaK122 and AsP122, respectively, which are significantly smaller than the BCS weak coupling limit of $2\Delta/k_BT_c = 3.52$. In particular, it is striking that $2\Delta/k_BT_c$ in BaK122 is smaller than that of AsP122 and is only half the value of the BCS limit. Such a small gap ratio of the hole bands in BaK122 system implies the multi-gap superconductivity with the electron pairing between disconnected FSs (S12). In this picture, small density of states (DOS) on one FS reflects in the small SC gap magnitude on the other, regardless of the nature of the pairing glue. According to the band calculations on BaK122, DOS in each hole FS is larger than that in each electron FS (S13). Small SC gap in hole FSs observed by laser-ARPES thus suggests the electron pair scattering between hole and electron FSs. This also implies that the electron bands have a larger gap ratio than hole bands, which can account for point contact Andreev reflection (S14) and lower critical field (S15) measurements reporting two-gap superconductivity in BaK122, where the smaller gap size actually well corresponds to that obtained by laser-ARPES.

5. Variation in the SC gap size in previous ARPES on BaK122

In the previous ARPES (S16-S19), hole FSs around zone center were resolved into only two bands, inner and outer. FS-sheet-dependence of the SC gap magnitude was reported as a two-gap structure; large SC gap around 9-12 meV (S16-S19) opens in inner hole FS (and electron FS around zone corner), while small gap of 6-8 meV

(S16,S17,S19) or less than 4 meV (S18) is observed in outer hole FS. Such variation of the gap values in each FS might be caused by imperfect SC gap opening in the ARPES spectra as pointed out in the previous report (S18).

The two-peak structure presently observed is one reason why the estimation of gap values near E_F has some variation among different groups in the previous ARPES (S16-S19) including recent hν-dependent measurements on BaK122 (S20,S21). The SC peak 1 might be easily integrated as a shoulder on the leading edge formed by peak 2, when the energy resolution is insufficient. Considering the binding energy of the peak positions (peak 1: ~5 meV, peak 2: ~12 meV), some of previous ARPES on BaK122 probably estimated the SC gap magnitude from the binding energy of non-SC peak 2. The bulk-sensitive and high-resolution laser-ARPES now enables us to extract genuine SC gap magnitude from the complex ARPES spectra of BaK122.

6. SC gap magnitude near $k_z = 0$ in AsP122

By employing Helium discharge lamp (hν = 21.2 eV), we observed hole FS around zone center and SC gap. Relatively small hole FS (Fig.2 **A**) indicates that k_z value corresponding to hν = 21.2 eV is near $k_z = 0$ rather than $k_z = \pi$ (Fig. S2 **C**). We also found that SC gap magnitude is almost identical to that taken by hν = 7 eV. This result indicates that at least at the representative two k_z values, SC gap variation in AsP122 is negligible. Recent hν-dependent ARPES on AsP122 shows that SC gap magnitude in hole FSs are almost the same at several k_z values between 0 and π (T. Yoshida et al., private communications). These results suggest that comparable SC gap magnitude in hole FSs is entirely/truly independent of the k_z value in AsP122.

7. Material dependence of the SC gap magnitude in hole FSs.

As shown in Fig. S3, typical SC gap magnitude estimated by the edge in the symmetrized spectra is 7 meV, 6 meV and 4.5 meV for FeCo122, AsP122 and BaK122, respectively. According to S12, such material dependence is explained by the electron pair scattering between disconnected hole and electron FSs. In this scenario, small density of states (DOS) on one FS reflects in the small SC gap magnitude on the other. Comparing between $Ba(Fe,Co)_2As_2$ (FeCo122), AsP122 and BaK122 systems, DOS in electron FSs around the zone corners become smaller from FeCo122 to BaK122, reflecting the decrease of electron density. It thus explains smaller SC gap magnitude in hole FS of BaK122 and systematic material dependence among three materials. While above discussion is independent of the nature of the pairing glue, dominant electron scattering along (π,π) direction suggests spin and/or orbital fluctuations originated in the FS nesting, rather than conventional electron-phonon mechanism.

8. Orbital character of the outer FS in AsP122

According to ref. S24, outer hole FS in AsP122 is dominantly composed of $3Z^2$-R^2 orbital near $k_z = \pi$. However, we note that there is an ambiguity of orbital character in the band calculations at $k_z = \pi$ of 122 system. In ref. S25, $3Z^2$-R^2 orbital disappears and is switched into X^2-Y^2 orbital at $k_z = \pi$ in Ba122. In order to discuss the orbital-independent SC gaps, here we experimentally check the orbital characters, especially focusing on the X^2-Y^2 and $3Z^2$-R^2 orbitals.

As shown in Figure S4 **A** and **B**, we performed polarization-dependent ARPES for sample geometries A and B. Each geometry corresponds to the measurement along the momentum cut illustrated in **D** and **E**, respectively. Selection rule for ARPES indicates that orbitals of even parity are detectable only by the light polarization of even parity (S26, S27). In both geometries A and B, s polarization is active for even parity orbitals with respect to the mirror planes, although p-polarization is summation of the even and odd parity. By comparing the results of s-polarization for geometries A and B, we can rule out one of the X^2-Y^2 and $3Z^2$-R^2 orbital characters according to the table in Fig2. **C**.

MDCs near E_F taken by s-polarization (**F** and **G**) clearly show the k_F peaks of outer hole FS in both geometries. According to the table in **C**, we can thus rule out X^2-Y^2 orbital character in outer hole FS of AsP122. This result is consistent with calculation by Kuroki et al., reporting dominant $3Z^2$-R^2 orbital component in outer hole FS near $k_z = \pi$ of AsP122 (S24).

Figure S1

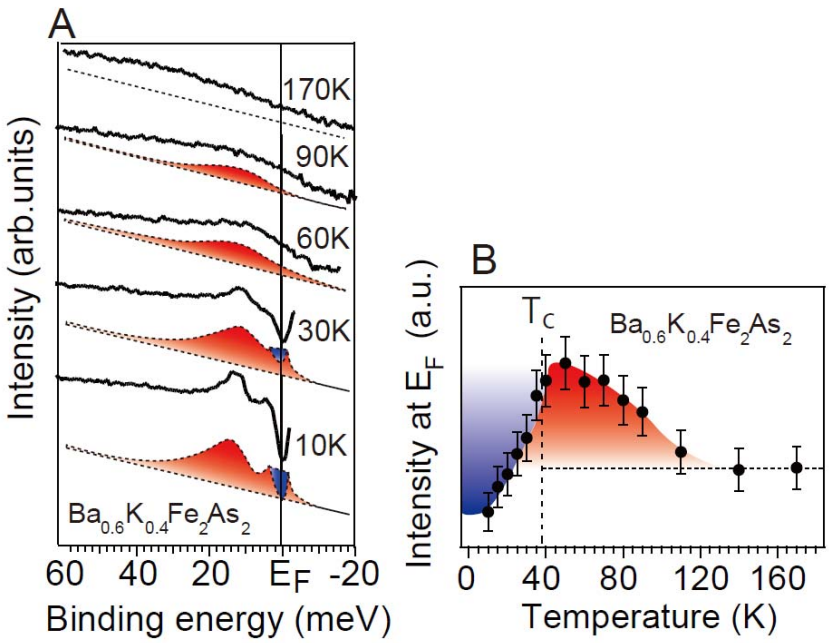

T. Shimojima et al.

Fig S1: (A) *T*-dependence of the EDCs divided by FD functions and its schematics. Colored in red and blue represent the peak 2 and the gap structure between peak 1 and 1', respectively. (B) *T*-dependence of the spectral intensity at E_F. Colored in red and blue represent the increasing spectral weight due to the evolution of peak 2 toward low-*T* and SC gap opening below T_c, respectively.

Figure S2

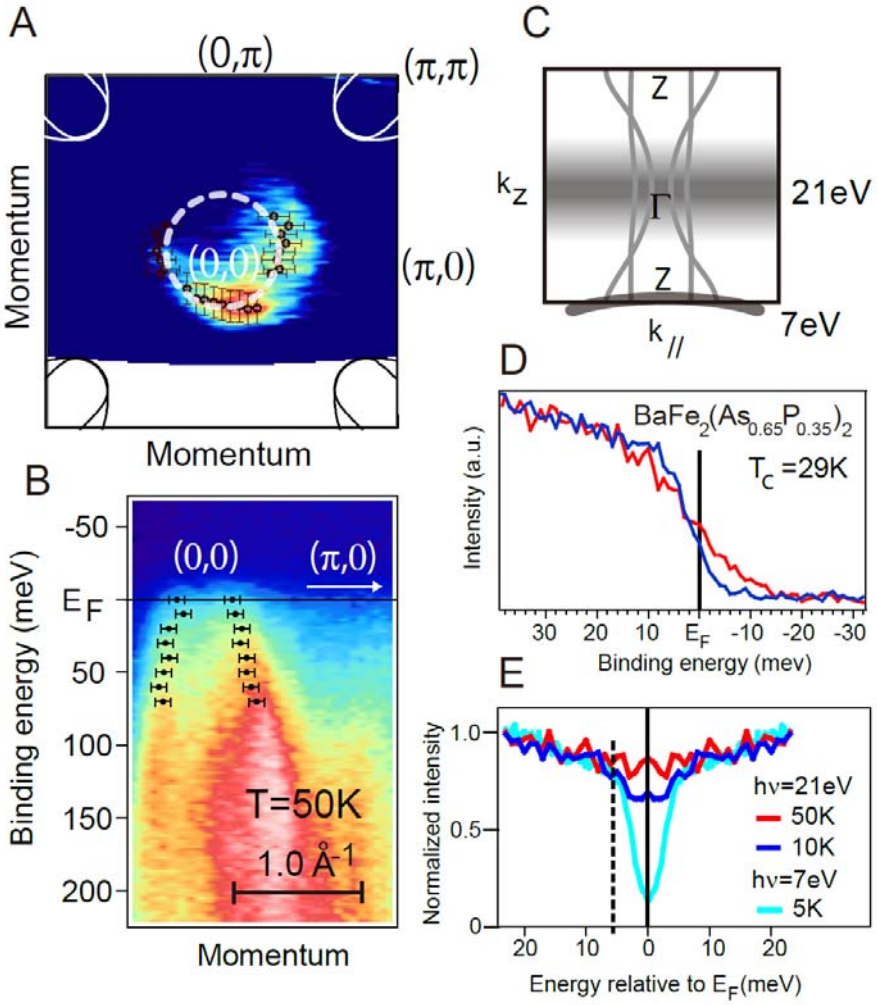

T. Shimojima et al.

Fig S2: (A) Hole FS around zone center measured by hv = 21.2 eV. Black symbols indicate FS crossing and the circle depicted by the broken curve represents a guide for the eyes of FS shape. Note that size of the hole FS is apparently smaller than that obtained by 7 eV photons. (B) Band dispersions along (0,0) – (π,0) cut. (C) Schematic

profile of the FSs along k_z taken from ref.S22. Momentum region measured by 21.2 eV is estimated to be within the gray area considering the small size of the hole FS. (D) EDCs at the k_F of the hole band below and above T_c. (E) Symmetrized EDCs in D measured by hν = 21.2 eV above T_c (red), hν = 21.2 eV below T_c (blue) and hν = 7 eV below T_c (light blue). SC gap size was estimated by edge in the spectra (broken line). Although residual DOS at E_F is rather high for 21.2 eV, We note that the size of SC gap in energy is almost identical to that taken by hν = 7eV.

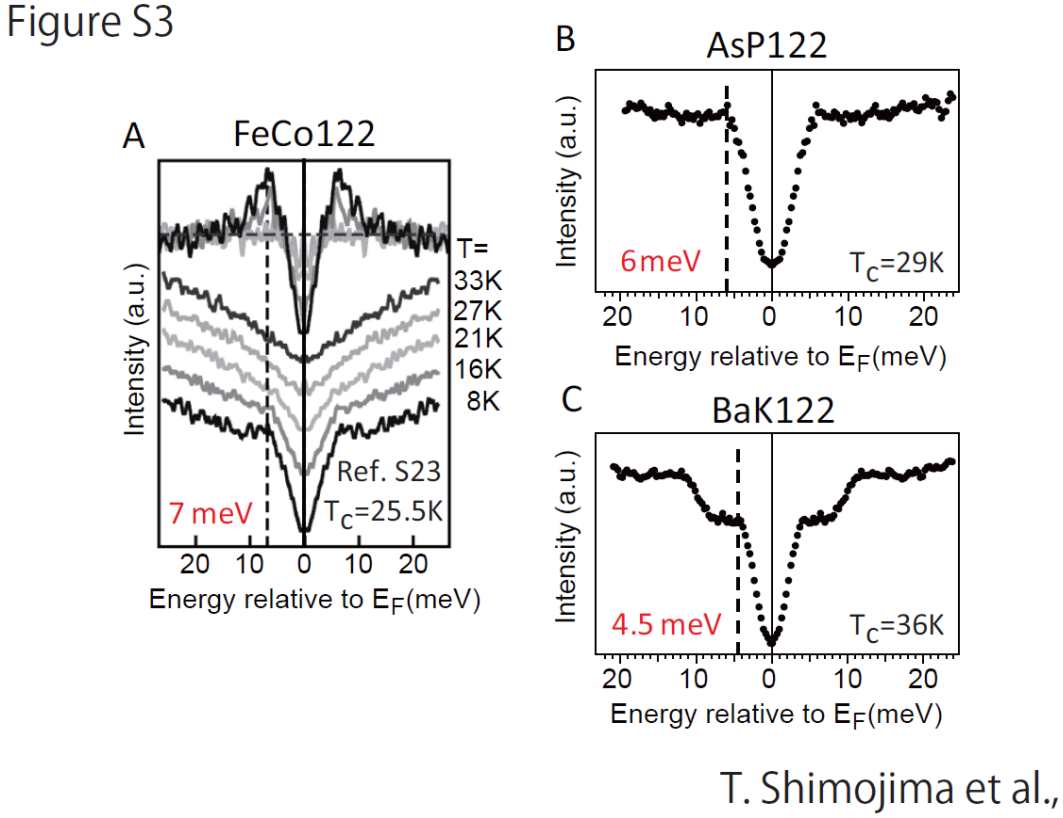

Figure S3: (**A** to **C**) Symmetrized SC gap spectra of FeCo122, AsP122 and BaK122, respectively. SC gap size is compared by the binding energy of the edge (broken line) in the symmetrized spectra. SC gap spectra of FeCo122 are taken from ref. S23, and those of AsP122 and BaK122 is obtained in this work.

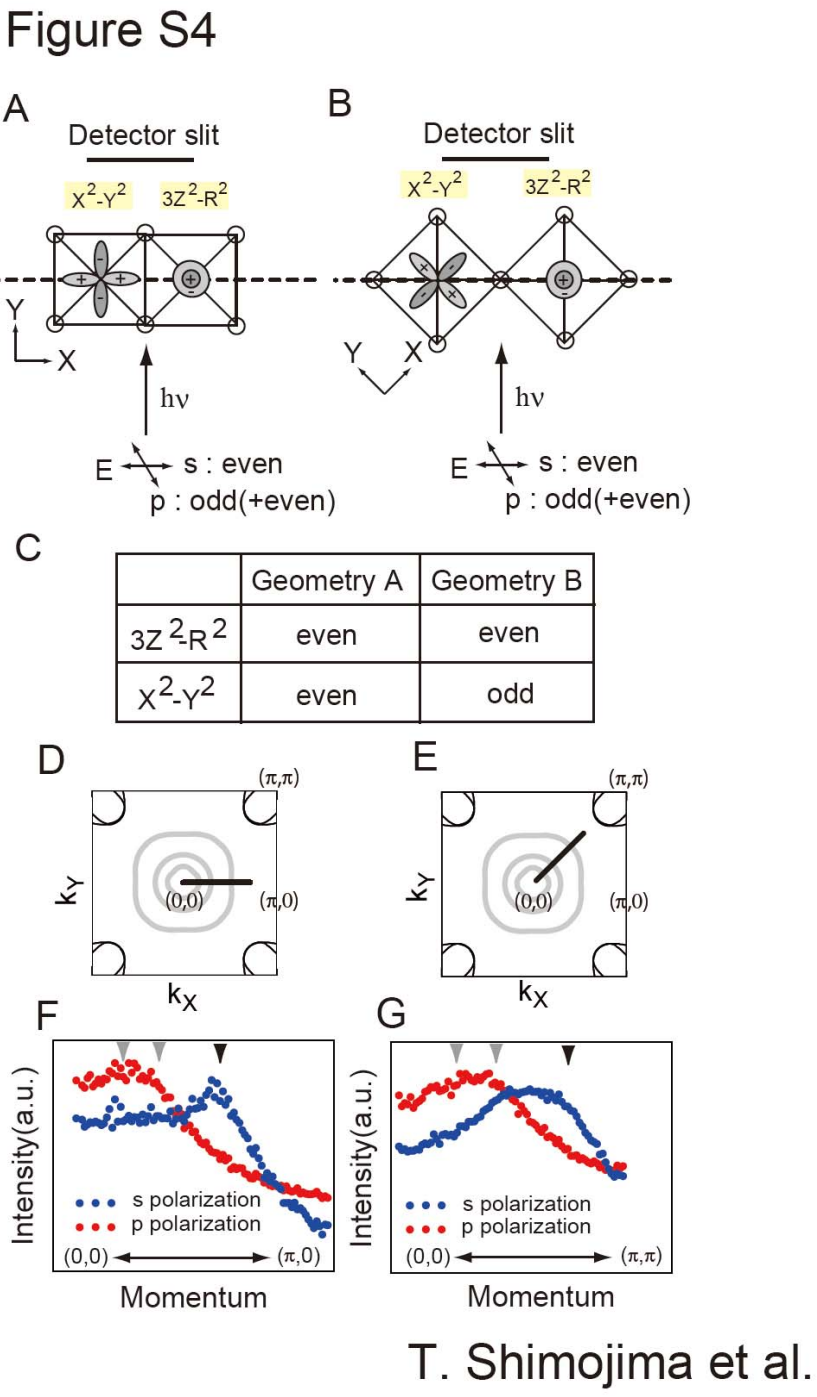

Fig S4: (**A** and **B**) Two experimental configurations for polarization-dependent laser-ARPES. Broken line represents the mirror plane of the crystal. Sample orientation

in A is rotated by 45 degrees from B. (**C**) Parity of $3Z^2$-R^2 and X^2-Y^2 orbitals with respect to the mirror plane in A (geometry A) and B (geometry B). (**D** and **E**) Momentum cuts measured in the geometries A and B, respectively. (**F** and **G**) Polarization dependence of MDC curves near E_F along (0,0)-(π,0) direction (geometry A) and (0,0)-(π,π) direction (geometry B), respectively. Arrows indicate k_F of inner (gray), middle (gray) and outer (black) hole bands estimated by laser-ARPES. Outer k_F is clearly observed by s-polarization in both geometries A and B.

Supporting References

S1. K. Kuroki *et al., Phys. Rev. B* **79**, 224511 (2009).

S2. M. P. Seah, W. A. Dench, *Surface And Interface Analysis* **1**, 2 (1979).

S3. T. Kiss,et al., *Review of Scientific Instruments* **79**, 023106 (2008).

S4. N. Katayama, Y. Kiuchi, Y. Matsushita, K. Ohgushi, *J. Phys. Soc. Jpn.* **78**, 123702 (2009).

S5. S. Kasahara, *et al., Phys. Rev. B* **81**, 184519 (2010)

S6. H. Matsui, *et al., Phys. Rev. Lett.* **90,** 217002 (2003).

S7. A. Loeser, *et al., Science* **273**, 325 (1996).

S8. H. Ding, *et al., Nature* (London) **382**, 51 (1996).

S9. A. D. Christianson, *et al., Nature* **456**, 930 (2008).

S10. H. Ikeda, R. Arita, J. Kunes, *Phys. Rev. B* **82**, 024508 (2010).

S11. M. Yi, et al., <http://arxiv.org/abs/1011.0050> (2010).

S12. O. V. Dolgov, *et al., Phys. Rev. B* **79**, 060502 (2009).

S13. I. I. Mazin, J. Schmalian, *Physica C* **469**, 614-627 (2009).

S14. P. Szabó, *et al., Phys. Rev. B* **79**, 012503 (2009).

S15. C. Ren, *et al.*, *Phys. Rev. Lett.* **101**, 257006 (2008).

S16. H. Ding, et al., *Euro. Phys. Lett.* **83**, 47001 (2008).

S17. K. Nakayama, *et al., Euro. Phys. Lett.* **85**, 67002 (2009).

S18. D. V. Evtushinsky, *et al., Phys. Rev. B* **79**, 054517 (2009).

S19. L. Wray, *et al., Phys. Rev. B* **78**, 184508 (2008).

S20. Y.-M. Xu, *et al.,* <http://arxiv.org/abs/1006.3958> (2010).

S21. Y. Zhang, *et al.,* Physical Review Letters 105, 117003 (2010).

S22. T. Yoshida *et al.,* <http://arxiv.org/abs/1008.2080> (2010).

S23. K. Terashima et al., *Proceedings of the National Academy of Sciences,* **106**, 7330 (2009)

S24. K. Suzuki et al., , <http://arxiv.org/abs/1010.3542> (2010).

S25. S. Graser et al., *Phys. Rev. B* **81**, 214503 (2010).

S26. S. Hufner, Photoelectron Spectroscopy (Springer, Berlin,2003).

S27. A. Damascelli, Z. Hussain, and Z.-X. Shen, *Rev. Mod. Phys.* **75**, 473 (2003).